Taylor & Francis
Taylor & Francis Group

Theoretical analysis of the evolution from ignition kernel to flame ball and planar flame

Z. CHEN* and Y. JU

Department of Mechanical and Aerospace Engineering, Princeton University,
Princeton, NJ 08544, USA

Dynamics of flame kernel evolution with and without external energy addition has been investigated analytically and numerically. Emphasis is placed on the effects of radiation heat loss, ignition power and Lewis number on the correlation and transition between the initial flame kernel, the self-extinguishing flame, the flame ball, the outwardly propagating spherical flame and the propagating planar flame. The present study extends previous results by bridging the theories of the non-adiabatic stationary flame balls and travelling flames and allowing rigorous consideration of radiation heat losses. The results show that the effects of radiation heat loss play an important role in flame regimes and flame transition and result in a new isolated self-extinguishing flame. Furthermore, it is found that radiation heat losses significantly increase the critical ignition radius and result in three different dependences of the minimum ignition power on the Lewis number. Comparisons between the results from the transient numerical simulation and those from the quasi-steady state analysis show a good agreement. The results suggest that prediction of flame initiation without appropriate consideration of radiation is not acceptable.

Keywords: Radiation heat loss; Flame extinction; Flame initiation; Minimum ignition energy

1. Introduction

Understanding of flame initiation is important not only for fundamental combustion research but also for fire safety control and the development of low-emission gasoline and homogeneous charge compression ignition (HCCI) engines. When an external energy is locally deposited into a combustible mixture, there are four possible outcomes: an evolution from outwardly propagating spherical flame to planar flame; a stationary flame ball; a propagating self-extinguishing flame; or a decaying ignition kernel (partially burning hot pocket) [1–3]. The evolution of the flame kernel and the final outcome depends on the magnitude of energy addition, fuel concentration, radiation heat loss and transport and kinetic properties. Efficient flame initiation with minimum energy deposition and successful control of fire spreading highly depend on the understanding of the correlations between ignition kernels, flame balls, self-extinguishing flames and propagating spherical and planar flames, as well as the impacts of radiation intensity and the transport properties on the flame regime transitions.

It is well known that for an unstretched planar flame, radiation heat loss defines the lean and rich flammability limits of a fuel [4, 5]. If the planar flame is stretched, sub-limit flames

---

may exist when the Lewis number is below a critical value [6–8]. For the same reason, sub-limit flames also exist for curved flames such as spherical flames. It has been known since the work of Zel'dovich *et al.* [9] that a diffusion controlled stationary flame ball with a characteristic equilibrium radius (flame ball radius) can exist at a mixture concentration lower than the flammability limit. A stability analysis showed that the adiabatic flame balls are inherently unstable [10]. A small perturbation will cause the flame either to propagate inward and eventually extinguish or to propagate outward and evolve into a planar flame. The flame ball size is considered to be a critical parameter in controlling flame initiation [9–11]. It was in Ronney's microgravity experiments [1, 12–15] that stable flame balls and self-extinguishing flames were first observed. Theoretical and numerical studies of flame balls [16–18] demonstrated that radiation heat loss plays an important role in affecting the flame ball size and stability. A flame ball with large equilibrium radius can be stabilized by radiation heat loss. Recently, the self-extinguishing flames and self-wrinkling flames were studied by Bechtold *et al.* [19], and the effects of radiation heat loss were investigated. However, since these theoretical studies were only focused on the dynamics of separated phenomena such as flame balls and self-extinguishing flames, the travelling flames were isolated from flame balls and self-extinguishing flames. As a result, the relation between self-extinguishing flames and flame balls and the relation between flame ball size and successful flame initiation of outwardly propagating flames were not well understood.

Recognizing the importance of the missing relationship between flame balls and travelling flames, a theoretical analysis by He and Law [3] was conducted to examine the transition of a propagating spherical flame to a flame ball. Although it was concluded that radiation heat loss has a significant effect on flame transition, the impact of radiation heat loss in the unburned region was not considered. In order further to examine the effect of detailed chemistry and transport properties on the flame transition between travelling flames and flame balls, numerical simulations were conducted for hydrogen–air mixtures at normal and elevated pressures [20, 21]. The results confirmed the existence of flame transition predicted by theory and provided quantitative comparison with experimental data. Because of the tremendous computation cost of travelling flames, the numerical simulations were unfortunately only limited to hydrogen mixtures. The effects of Lewis number on the flame transition and the different contributions of radiation heat losses from burned and unburned zones on the flame transitions remain unclear. A recent study by He [22] was motivated to study the flame initiation at large Lewis numbers, but it did not consider radiation heat loss. This makes the results less realistic because near limit flame initiation is dominantly affected by radiation heat loss. Therefore, the role of the heat loss on flame transition and the correlation between the flame regimes from ignition kernels to flame balls and propagating flames remain unknown.

The present study is aimed at: (a) providing a general theoretical description of the flame transition between the initial flame kernel, the self-extinguishing flame, the flame ball and the outwardly propagating flame; and (b) bridging both the flame ball theory and the travelling flame theory with specific emphasis on the effects of Lewis number and the individual contribution of radiation heat losses from burned and unburned zones on the flame regimes, flame transition and minimum flame initiation energy and kernel size. First, the mathematical model is given. Then, based on the quasi-steady assumption, an analytical expression describing the flame propagating speed is obtained and validation in limiting cases is demonstrated. The effects of radiation heat losses on flame regimes and flame transition, and ignition energy effects on flame initiation are studied. Finally, numerical simulation of the time-dependent flame initiation problem is conducted to verify the theoretical results.

2. Mathematical model

We consider an unsteady spherical flame kernel evolution with and without an external ignition source at the centre. By assuming constant thermal properties, the conservation equations for energy and fuel mass are given as

$$\tilde{\rho}\tilde{C}_P \frac{\partial \tilde{T}}{\partial \tilde{t}} = \frac{1}{\tilde{r}^2} \frac{\partial}{\partial \tilde{r}}\left(\tilde{r}^2 \tilde{\lambda}\frac{\partial \tilde{T}}{\partial \tilde{r}}\right) - \tilde{H} + \tilde{q}\tilde{\omega} \tag{1a}$$

$$\tilde{\rho}\frac{\partial \tilde{Y}}{\partial \tilde{t}} = \frac{1}{\tilde{r}^2}\frac{\partial}{\partial \tilde{r}}\left(\tilde{r}^2 \tilde{\rho}\tilde{D}\frac{\partial \tilde{Y}}{\partial \tilde{r}}\right) - \tilde{\omega} \tag{1b}$$

where $\tilde{t}, \tilde{r}, \tilde{\rho}, \tilde{T}$ and $\tilde{Y}$ are time, radial coordinate, density, temperature and fuel mass fraction, respectively. $\tilde{q}$ is the reaction heat-release per unit mass of fuel, $\tilde{C}_P$ is the specific heat capacity at constant pressure, $\tilde{\lambda}$ is the thermal conductivity and $\tilde{D}$ is the mass diffusivity of fuel. To simplify the problem in the theoretical analysis, we also adopt the commonly used constant density model [23] so that the convection flux is absent. The validation of this assumption will be made later by transient numerical simulation. $\tilde{\omega}$ is the reaction rate for one-step irreversible reaction, $\tilde{\rho}\tilde{A}\tilde{Y}\exp(-\tilde{E}/\tilde{R}^0\tilde{T})$, in which $\tilde{A}$ is the pre-factor of Arrhenius law, $\tilde{E}$ the activation energy, and $\tilde{R}^0$ the universal gas constant. The volumetric radiation heat loss $\tilde{H}$ is estimated by using the optically thin model, $\tilde{H} = 4\tilde{\sigma}\tilde{K}_p(\tilde{T}^4 - \tilde{T}_\infty^4)$, where $\tilde{\sigma}$ is the Stefan–Boltzmann constant and $\tilde{K}_p$ denotes the Planck mean absorption coefficient of the mixture.

By using the adiabatic planar flame speed $\tilde{S}_L^0$ and the flame thickness $\tilde{\delta}_f^0 = \tilde{\lambda}/\tilde{\rho}\tilde{C}_P\tilde{S}_L^0$, the velocity, length, time, temperature and fuel mass fraction can be normalized as

$$u = \frac{\tilde{u}}{\tilde{S}_L^0} \quad r = \frac{\tilde{r}}{\tilde{\delta}_f^0} \quad t = \frac{\tilde{t}}{\tilde{\delta}_f^0/\tilde{S}_L^0} \quad T = \frac{\tilde{T} - \tilde{T}_\infty}{\tilde{T}_{ad} - \tilde{T}_\infty} \quad Y = \frac{\tilde{Y}}{\tilde{Y}_\infty} \tag{2}$$

where $\tilde{T}_\infty$ and $\tilde{Y}_\infty$ denote the temperature and fuel mass fraction in the fresh mixture, and $\tilde{T}_{ad} = \tilde{T}_\infty + \tilde{Y}_\infty \tilde{q}/\tilde{C}_P$ is the adiabatic flame temperature of planar flame. By further attaching the coordinate to the moving flame front, $R = R(t)$, the non-dimensional equations take the following form

$$\frac{\partial T}{\partial t} - U\frac{\partial T}{\partial r} = \frac{1}{r^2}\frac{\partial}{\partial r}\left(r^2\frac{\partial T}{\partial r}\right) - H + \omega \tag{3a}$$

$$\frac{\partial Y}{\partial t} - U\frac{\partial Y}{\partial r} = \frac{Le^{-1}}{r^2}\frac{\partial}{\partial r}\left(r^2\frac{\partial Y}{\partial r}\right) - \omega \tag{3b}$$

where $Le = \tilde{\lambda}/\tilde{\rho}\tilde{C}_P\tilde{D}$ is the Lewis number and U the flame front propagating speed, $U(t) = dR(t)/dt$. The radiation heat loss and chemical reaction rate are normalized, respectively, as

$$H = \frac{\tilde{H}\tilde{\delta}_f^0}{\tilde{\rho}\tilde{C}_P\tilde{S}_L^0(\tilde{T}_{ad} - \tilde{T}_\infty)} \quad \omega = \frac{\tilde{\omega}\tilde{\delta}_f^0}{\tilde{\rho}\tilde{S}_L^0\tilde{Y}_\infty} \tag{4}$$

It can be seen that the present model extends the previous theoretical flame ball models [9, 16, 17] by including travelling flames and radiation heat loss on both the burned and unburned sides, so that the correlation between flame ball and travelling flames and the impact of radiation on the flame transition between different flame regimes can be qualitatively examined.

In the limit of large activation energy, chemical reaction occurs only within a very thin zone of high temperature and the reaction rate can be replaced by a Delta function with jump

conditions used at the flame front [23]

$$\omega = \exp\left[\frac{Z}{2}\frac{T_f - 1}{\sigma + (1 - \sigma)T_f}\right] \cdot \delta(r - R) \tag{5}$$

where $Z = \tilde{E}(1 - \sigma)/\tilde{R}^0\tilde{T}_{ad}$ is the Zel'dovich number and $\sigma = \tilde{T}_\infty/\tilde{T}_{ad}$ the expansion ratio. The jump relations at the flame interface becomes

$$\left.\frac{dT}{dr}\right|_{R^-} - \left.\frac{dT}{dr}\right|_{R^+} = \frac{1}{Le}\left(\left.\frac{dY}{dr}\right|_{R^+} - \left.\frac{dY}{dr}\right|_{R^-}\right) = \exp\left[\frac{Z}{2}\frac{T_f - 1}{\sigma + (1 - \sigma)T_f}\right] \tag{6}$$

In the present study, we also examine the impact of external energy deposition on successful flame initiation and flame transition. A constant energy flux is locally deposited in an initially homogeneous mixture. For an initial flame kernel with a radius of R, the centre of the flame kernel is located at $r = 0$, and $0 \leq r \leq R$ and $R \leq r < \infty$ are respectively the burned and unburned regions. By defining the flame as the location where fuel concentration goes to zero, the boundary conditions for temperature and fuel mass fraction can be given as

$$r = 0, \quad r^2\partial T/\partial r = -Q, \quad Y = 0 \tag{7a}$$

$$r = R, \quad\quad\quad T = T_f, \quad Y = 0 \tag{7b}$$

$$r = \infty, \quad\quad\quad T = 0, \quad Y = 1 \tag{7c}$$

where Q is the normalized ignition power given by

$$Q = \frac{\tilde{Q}}{4\pi\tilde{\lambda}\tilde{\delta}_f^0(\tilde{T}_{ad} - \tilde{T}_\infty)} \tag{8}$$

3.   Theoretical analysis

The unsteady problem given by equations (3a) and (3b) cannot be solved analytically. In fact, as will be demonstrated later by unsteady numerical simulations, it is reasonable to assume that in the attached coordinate moving with flame front, the flame can be considered as in quasi-steady state ($\partial/\partial t = 0$). This assumption has been widely used in previous studies [10, 22, 24]. Therefore, the governing equations can be simplified to

$$-U\frac{dT}{dr} = \frac{1}{r^2}\frac{d}{dr}\left(r^2\frac{dT}{dr}\right) - h \cdot T + \omega \tag{9a}$$

$$-U\frac{dY}{dr} = \frac{Le^{-1}}{r^2}\frac{d}{dr}\left(r^2\frac{dY}{dr}\right) - \omega \tag{9b}$$

In addition, for the convenience of the algebraic manipulation the heat loss term H is approximated by a linear function of normalized temperature as $H = h \cdot T$ and h is the heat loss constant which takes the following form

$$h = \frac{4\tilde{\sigma}\tilde{K}_P\tilde{\delta}_f^0(\tilde{T}^4 - \tilde{T}_\infty^4)}{\tilde{\rho}\tilde{C}_P\tilde{S}_L^0(\tilde{T} - \tilde{T}_\infty)} \approx \frac{4\tilde{\sigma}\tilde{K}_P\tilde{\lambda}}{\left(\tilde{\rho}\tilde{C}_P\tilde{S}_L^0\right)^2}\tilde{T}_{ad}^3 \tag{10}$$

Note that the radiation heat loss constant involves the radiation intensity and the fuel concentration. For any given mixture composition, an increase of h means a decrease of fuel concentration (decrease of flame speed). For methane–air flames, the heat loss constant h calculated according to equation (10) is in the range of 0.001 to 0.1.

3.1 *Analytical solution without external energy addition*

Equation (9) with boundary conditions given by equation (7) can be solved analytically for $Q = 0$. An exact solution of temperature and fuel mass fraction distribution can be found. For fuel lean cases, the fuel mass fraction in burned gas region ($0 \leq r \leq R$) is zero and that in unburned gas region ($R \leq r < \infty$) is obtained by solving equation (9b) with boundary conditions given by equations (7b) and (7c).

$$Y(r) = 1 - \int_r^\infty \frac{e^{-ULe\tau}}{\tau^2} d\tau \bigg/ \int_R^\infty \frac{e^{-ULe\tau}}{\tau^2} d\tau \quad \text{for } r \geq R \qquad (11)$$

As to the temperature distribution, for adiabatic flames ($h = 0$), the analytical solution is

$$T(r) = \begin{cases} T_f & \text{for } 0 \leq r \leq R \\ T_f \int_r^\infty \frac{e^{-U\tau}}{\tau^2} d\tau \bigg/ \int_R^\infty \frac{e^{-U\tau}}{\tau^2} d\tau & \text{for } r \geq R \end{cases} \qquad (12)$$

For non-adiabatic flames, since the radiation properties in burned and unburned gases may be different, we use h_1 and h_2 to represent the heat loss constants in the burned and unburned regions, respectively, in order to examine the individual contribution of the radiation heat losses from these two regions. By defining $k_i = \sqrt{U^2 + 4h_i}$ ($i = 1, 2$), an analytical solution of temperature distribution is obtained

$$T(r) = \begin{cases} T_f \cdot e^{[0.5(U+k_1)(R-r)]} \dfrac{F(k_1 r, U/k_1, -U/k_1)}{F(k_1 R, U/k_1, -U/k_1)} & \text{for } 0 \leq r \leq R \\ T_f \cdot e^{[0.5(U+k_2)(R-r)]} \dfrac{G(-k_2 r, U/k_2, -U/k_2)}{G(-k_2 R, U/k_2, -U/k_2)} & \text{for } r \geq R \end{cases} \qquad (13)$$

where

$$F(a, b, c) = \int_0^1 e^{at} t^b (1-t)^c dt$$

and

$$G(a, b, c) = \int_0^\infty e^{at} t^b (1+t)^c dt.$$

Note that this exact solution removes the requirement of small heat loss assumption ($h \sim 1/Z \leq 1$) which is commonly used in the previous studies [16, 17, 23]. Therefore, the present study provides a more rigorous consideration of radiation modelling to understand the relation between the spherical flames and the far field propagating planar flames in the limit of $R \to \infty$.

By using jump relations given by equation (6), one obtains an algebraic system of equations for flame propagating speed U, flame radius R and flame temperature T_f

$$\Omega \cdot T_f = \frac{1}{Le} R^{-2} e^{-ULeR} \bigg/ \int_R^\infty \tau^{-2} e^{-ULe\tau} d\tau = \exp\left[\frac{Z}{2} \frac{T_f - 1}{\sigma + (1-\sigma)T_f}\right] \qquad (14a)$$

where

$$
\Omega = \begin{cases}
R^{-2}e^{-UR} \Big/ \displaystyle\int_R^\infty \tau^{-2}e^{-U\tau}d\tau & \text{if } h_1 = 0, h_2 = 0 \\[4mm]
-\dfrac{U+k_1}{2} + k_1\dfrac{F(k_1R, 1+U/k_1, -U/k_1)}{F(k_1R, U/k_1, -U/k_1)} & \text{if } h_1 \neq 0, h_2 = 0 \\[4mm]
\quad + R^{-2}e^{-UR} \Big/ \displaystyle\int_R^\infty \tau^{-2}e^{-U\tau}d\tau & \\[4mm]
T_f\dfrac{U+k_2}{2} + T_fk_2\dfrac{G(-k_2R, 1+U/k_2, -U/k_2)}{G(-k_2R, U/k_2, -U/k_2)} & \text{if } h_1 = 0, h_2 \neq 0 \\[4mm]
\dfrac{k_2-k_1}{2} + k_1\dfrac{F(k_1R, 1+U/k_1, -U/k_1)}{F(k_1R, U/k_1, -U/k_1)} & \text{if } h_1h_2 \neq 0 \\[4mm]
\quad + k_2\dfrac{G(-k_2R, 1+U/k_2, -U/k_2)}{G(-k_2R, U/k_2, -U/k_2)} &
\end{cases}
\tag{14b}
$$

Therefore, the present study extends the study of He [22] by considering the coupling of radiation heat loss with the flame kernel evolution, which is the key mechanism for near limit flames, and allows bridging between the spherical flame limits and the flammability limit of planar flames. By numerically solving equation (14), the relation between flame propagating speed, flame radius and flame temperature and the existence of different flame regimes at different radiation heat loss constants (or different fuel concentrations) and Lewis numbers can be obtained.

3.2 *Validation in limiting cases*

In the following it will be shown that, in different limiting cases, the current model recovers the previous results of stationary flame balls [16, 17], outwardly propagating spherical flames [24] and planar flames [4, 23].

3.2.1 Stationary flame ball. In previous studies [16, 17], the non-adiabatic stationary flame ball was investigated via asymptotic analysis assuming small heat loss ($h_1 = h_{in}/Z$, $h_2 = h_{out}/Z^2$) and the relation between heat loss and flame radius was obtained

$$
Ln\left(\frac{R}{R_Z}\right) = L_{in}\left(\frac{R}{R_Z}\right)^2 + L_{out}\left(\frac{R}{R_Z}\right)
\tag{15}
$$

where

$$
L_{in} = \frac{h_{in}}{6}\frac{R_Z^2 T_{fZ}}{[\sigma + (1-\sigma)T_{fZ}]^2}
$$

and

$$
L_{out} = \frac{\sqrt{h_{out}}}{2}\frac{R_Z T_{fZ}}{[\sigma + (1-\sigma)T_{fZ}]^2}.
$$

T_{fZ} and R_Z are flame temperature and radius of adiabatic stationary flame ball [9].

$$
T_{fZ} = \frac{1}{Le} \quad R_Z = \frac{1}{Le}\cdot\exp\left[-\frac{Z}{2}\frac{1-Le}{1-\sigma(1-Le)}\right]
\tag{16}
$$

In the present study, the exact solution for fuel mass fraction and temperature distribution is obtained without using small heat loss assumption. In the limit of $U = 0$, equation (14)

reduces to the following form for non-adiabatic stationary flame ball

$$T_f\sqrt{h_2} + T_f\frac{\sqrt{h_1}}{\tan h(\sqrt{h_1}R)} = \frac{1}{R \cdot Le} = \exp\left[\frac{Z}{2}\frac{T_f - 1}{\sigma + (1 - \sigma)T_f}\right] \tag{17}$$

If small heat loss assumption ($h_1 = h_{in}/Z, h_2 = h_{out}/Z^2$) is used and high-order terms of $1/Z$ are neglected, the above relation can be reduced to the same form as equation (15). Therefore, the flame ball solution [16, 17] is a limiting case of the present result.

3.2.2 Outwardly propagating spherical flames.

A flame speed relation for propagating spherical flames was obtained by Frankel and Sivashinsky [24]. It is readily seen that the present result given by equation (14) recovers the same result in the limit of zero heat loss and large flame radius ($h_1 = h_2 = 0$ and $R \gg 1$). Specifically, for $R \gg 1$, the exponential integral can be represented by an asymptotic series

$$R^{-2}e^{-ULeR} \bigg/ \int_R^\infty \tau^{-2}e^{-ULe\tau}d\tau \approx ULe + \frac{2}{R} \tag{18}$$

By using the above expansion and defining $V = U + 2/R$, equation (14) reduces to the following form

$$T_fV = V + \frac{2}{R}\left(\frac{1}{Le} - 1\right) = \exp\left[\frac{Z}{2}\frac{T_f - 1}{\sigma + (1 - \sigma)T_f}\right] \tag{19}$$

The following relation can be immediately derived from equation (19), which is exactly the same equation given by Frankel and Sivashinsky [24]

$$VLnV = \frac{Z}{R}\left(\frac{1}{Le} - 1\right) \tag{20}$$

As such, the present models are valid in both limits of flame ball and travelling flames and can provide the relationship and transition mechanism between these two flames during flame kernel growth.

3.2.3 Planar flame speed and flammability limit.

In the limit of $R \to \infty$, the functions F and G become

$$\frac{F(k_1R, 1 + U/k_1, -U/k_1)}{F(k_1R, U/k_1, -U/k_1)} \to 1 \quad \frac{G(-k_2R, 1 + U/k_2, -U/k_2)}{G(-k_2R, U/k_2, -U/k_2)} \to 0$$

Therefore, equation (14) reduces to

$$T_f\frac{k_1 + k_2}{2} = U = \exp\left[\frac{Z}{2}\frac{T_f - 1}{\sigma + (1 - \sigma)T_f}\right] \tag{21}$$

Asymptotically, when the heat loss is in the order of $1/Z$ in the limit of large Zel'dovich number ($h_1 = h_{in}/Z, h_2 = h_{out}/Z$, and $Z \gg 1$), equation (21) recovers the classical theory of flammability limit for planar flames [4, 23]

$$L = -U^2Ln(U^2) \quad \text{with} \quad L = h_{in} + h_{out} = Z(h_1 + h_2) \tag{22}$$

The flammability limit is defined by $L = 1/e$ and $U = e^{-1/2}$. Therefore, equation (14) is a general solution to describe the dynamics of flame kernel growth and depicts a clear correlation between the ignition kernel, flame ball, propagating curved flames and planar flames. In the following section, we will demonstrate the role of radiation heat loss, Lewis number and external energy addition in flame regimes and flame initiation.

3.3 *Effects of radiation heat losses from the burned and unburned regions*

Radiation heat losses from the burned and unburned zones affect the flame temperature in different ways. Heat loss from the unburned zone will directly reduce the flame temperature. However, heat loss from the burned region only affects the flame temperature via the heat conduction from the flame. In addition, the radiation heat loss depends on the ratio of high temperature volume and the flame front surface area. As the flame kernel grows, the ratio changes significantly. For example, the normalized radiation heat losses from burned and unburned zones can be given as

$$H_{in} = h_1 \int_0^R T(r) \cdot r^2 dr \left/ \left(R^2 \frac{dT}{dr}\bigg|_{R^-} - R^2 \frac{dT}{dr}\bigg|_{R^+} \right) \right. \tag{23a}$$

$$H_{out} = h_2 \int_R^\infty T(r) \cdot r^2 dr \left/ \left(R^2 \frac{dT}{dr}\bigg|_{R^-} - R^2 \frac{dT}{dr}\bigg|_{R^+} \right) \right. \tag{23b}$$

where $(R^2 \frac{dT}{dr}|_{R^-} - R^2 \frac{dT}{dr}|_{R^+})$ is the total heat generation from chemical reaction. By using the temperature distribution obtained in equation (13), the ratio of these heat losses in the limit of small and large flame radius becomes

$$\frac{H_{in}}{H_{out}} = \begin{cases} 0 & \text{if } R \to 0 \\ \dfrac{h_1}{h_2} \cdot \dfrac{\sqrt{1 + 4h_2/U^2} + 1}{\sqrt{1 + 4h_1/U^2} - 1} & \text{if } R \to \infty \end{cases} \tag{24}$$

The above qualitative result shows that the radiation heat losses from burned and unburned zones will have different impact on flame temperature and flame transition. Unfortunately, in previous theoretical studies [3, 22], the radiation heat loss in the unburned region was simply neglected and the competing role of radiation heat losses from the unburned and burned zones as the flame kernel grows were not well understood.

In the following we will take an example of CH_4-air flames and use equation (14) to demonstrate how differently the radiation heat losses from the burned and unburned regions affect the flame temperature and speed. For flames around stoichiometric equivalence ratio, we choose $Z = 10$ and $\sigma = 0.15$. Equation (23) is used to evaluate the radiation heat losses from different zones and the total normalized radiation heat loss is the summation of them $H_{all} = H_{in} + H_{out}$.

Figure 1 shows the dependence of normalized heat loss and flame propagating speed on the flame radius for $Le = 1$ and $h = 0.015$. It is seen that there are two branches in the $U - R$ diagram: the fast stable branch *abc* and the slow unstable branch *cde*. At point *c*, the flame is extinguished at a finite propagating speed because the normalized heat loss reaches its maximum on the fast flame branch *abc*. It is also observed that the normalized total heat loss changes non-monotonically as the flame radius increases. There exists a minimum value as the flame reaches point *b* for fast branch and point *d* for slow branch. This phenomenon can only be explained by considering the individual contributions of heat losses in the burned and unburned zones.

The dependences of the normalized radiation heat losses in the burned and unburned zones, H_{in} and H_{out}, are shown in figure 1(b). It is seen that H_{in} increases monotonically with flame radius while H_{out} decreases monotonically with flame radius. It is shown that the radiation heat loss from the unburned zone H_{out} remains nearly constant when flame radius is larger than 20 and it is one order smaller than H_{in} ($H_{out}/H_{in} < 0.1$ when $R > 20$). This means that the effect of heat loss in the unburned zone becomes weaker as the flame grows, but it does not mean that the heat loss from the unburned zone can be neglected because heat losses from these zones affect flame temperature in different ways. The rapid increase of flame speed and
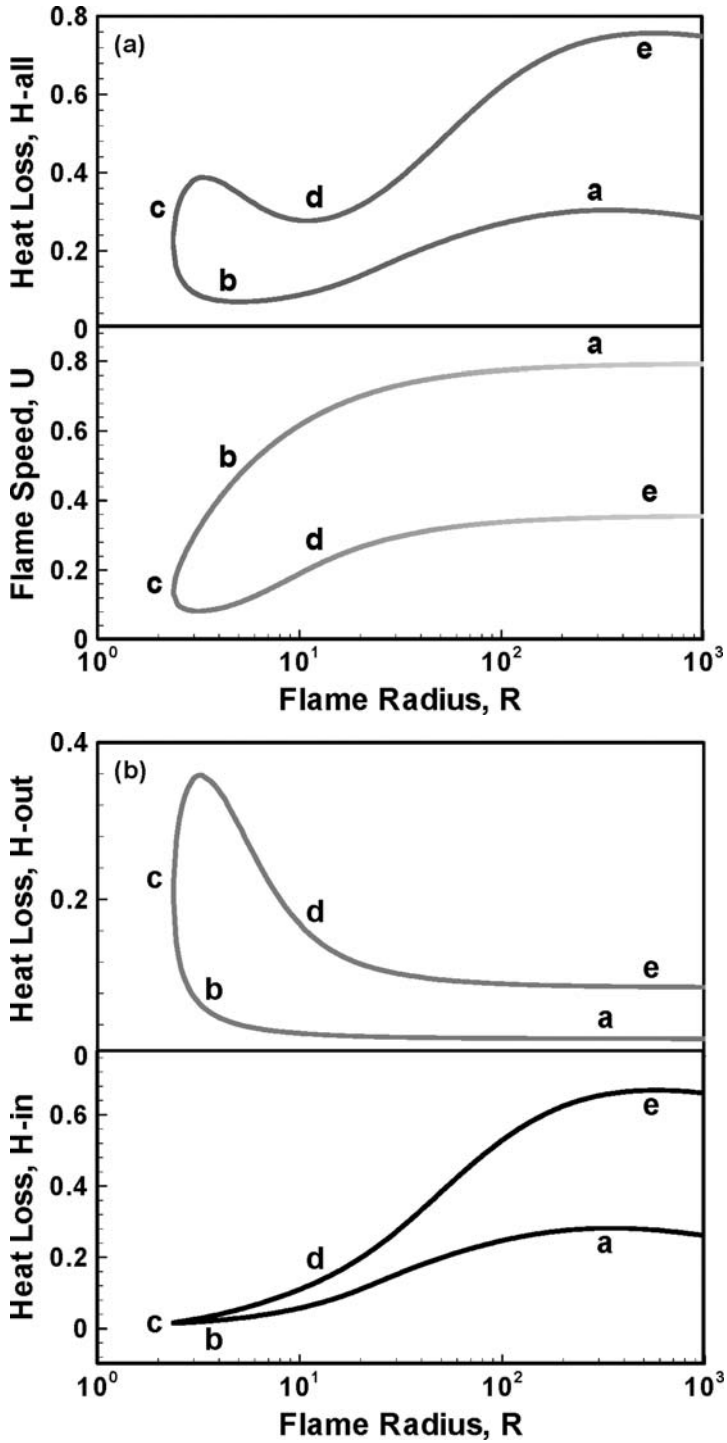
Figure 1. The dependence of normalized radiation heat loss and flame propagating speed on flame radius for $Le = 1$ and $h = 0.015$: (a), $H_{all} - R$ and $U - R$; (b), $H_{in} - R$ and $H_{out} - R$.

the peak of the radiation heat loss in the region of $R < 20$ are caused by the competition of radiation heat losses from the burned and unburned zones.

For the radiation heat loss larger than the critical heat loss ($L = 1/e$ and $h_c = 0.0184$) of the flammability of the planar flame, a flame will not exist at large flame radius. Figure 2 shows the dependences of normalized heat loss and flame propagating speed on the flame radius for $Le = 1$ and $h = 0.0197$. It is interesting to note that propagating spherical flame still exists at intermediate flame radii and there are two extinction limits, respectively, at small and large radii. The normalized total heat loss also changes non-monotonically and peaks at both extinction limits. This indicates that the extinction at small radius is caused by the heat loss in the unburned zone and the extinction at large radius by that from the burned zone [figure 2(b)]. The appearance of the extinction limit at small flame radius has not been reported in previous studies and the existence of this extinction limit will significantly affect the ignition kernel size for successful flame initiation. Therefore, in order to understand the flame kernel evolution adequate inclusion of the effect of radiation heat loss in the unburned gas is particularly important.

3.4 *Correlation between different flame regimes at different Lewis numbers*

Figure 3(a) shows the flame propagating speed as a function of flame radius for various radiation heat loss constants (or different fuel concentrations) with $Le = 1$. To demonstrate further the importance of heat loss in the unburned zone, the results with radiation heat loss only from the burned gas is shown in figure 3(b). In figure 3, solutions on the horizontal axis of $U = 0$ denote the stationary flame balls [equation (17)] and those on the vertical axis at large flame radius denote the planar flame [equation (21)]. The solution curves between the flame ball solutions and the planar flame solutions represent the travelling spherical flames. It is seen from figure 3(a) that for adiabatic flame ($h = 0$), the quasi-steady state flame ball exists at small radius. As the flame size grows the flame speed increases rapidly because of the increase of diffusion flux and eventually reaches the planar flame speed ($U = 1$) at a large flame radius. When there is a small radiation heat loss ($h = 0.005$), the quasi-steady state flame ball solution does not exist, and at a small flame radius, flame extinguishes at a finite flame speed. As the flame radius increases, flame speed increases and ultimately reaches the corresponding non-adiabatic planar flame speed. As the radiation heat loss further increases and becomes larger than the critical heat loss associated with the flammability limit, as explained in figure 2(a), sub-limit flames only exist at intermediate sizes and the radiation heat losses from the unburned and burned zones yield two extinction limits at small and large flame radii, respectively. To distinguish this flame regime from the self-extinguishing flame observed in the microgravity experiments [1, 13], we will refer to it as an isolated self-extinguishing flame because this flame cannot be initiated by a small localized ignition source. When only the radiation heat loss in the burned zone is considered [figure 3(b)], it is seen that the quasi-steady state solution of stationary flame ball exists for all heat losses. This obviously contradicts to the experimental observation [14]. Therefore, it can be concluded that the present model can successfully predict the existence of multiple flame regimes and the transition between the flame ball and travelling flame. Radiation from the unburned zone yields a new flame island at intermediate flame radii. The exclusion of radiation heat loss from unburned zone prevents correct prediction of the flame regimes and their transitions.

The flame speed dependences on flame radius for $Le = 0.8$ and 1.2 are shown in figures 4(a) and 5(a), respectively. For comparison, the results without radiation heat loss in the unburned zone are shown in figures 4(b) and 5(b). The effects of Lewis number on the flame regime and the flame transition can be found by comparing the results with figure 3. It can be seen
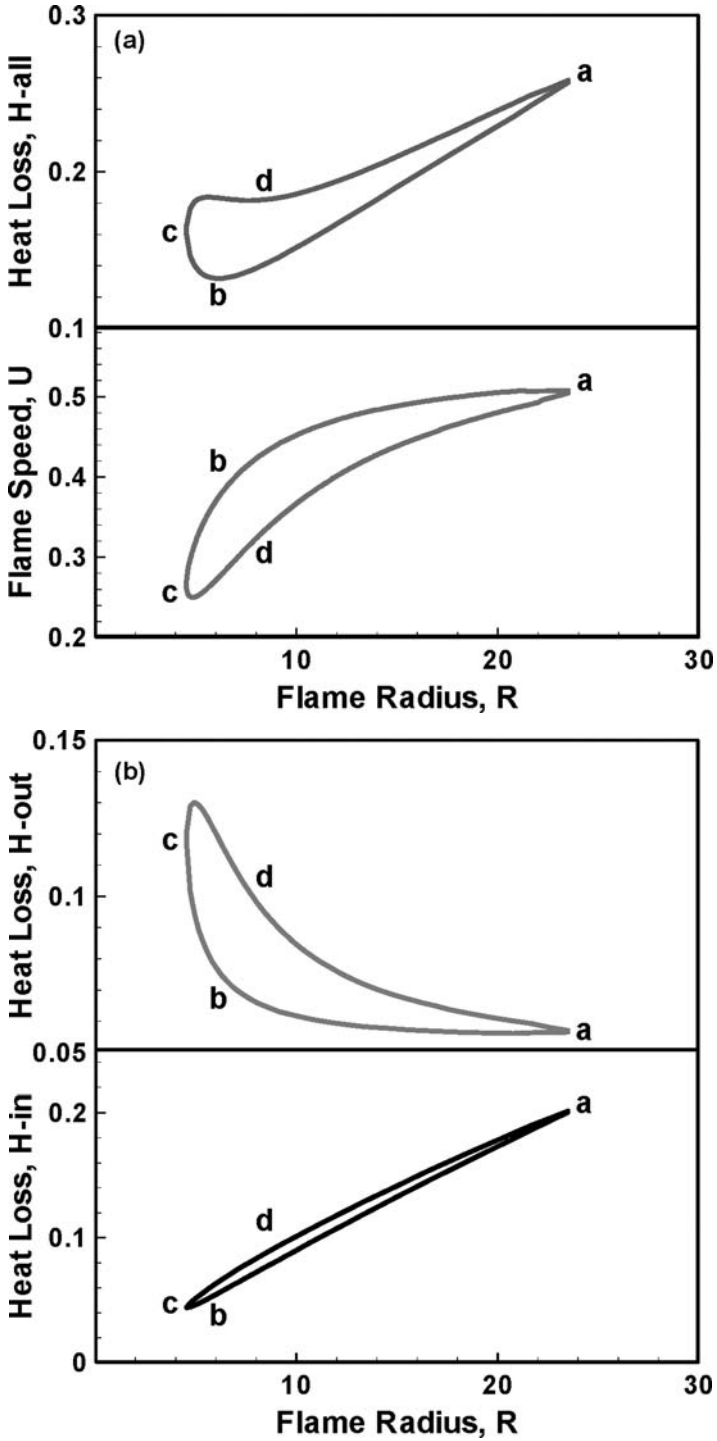
Figure 2. The dependence of normalized radiation heat loss and flame propagating speed on flame radius for $Le = 1$ and $h = 0.0197$: (a), $H_{all} - R$ and $U - R$; (b), $H_{in} - R$ and $H_{out} - R$.
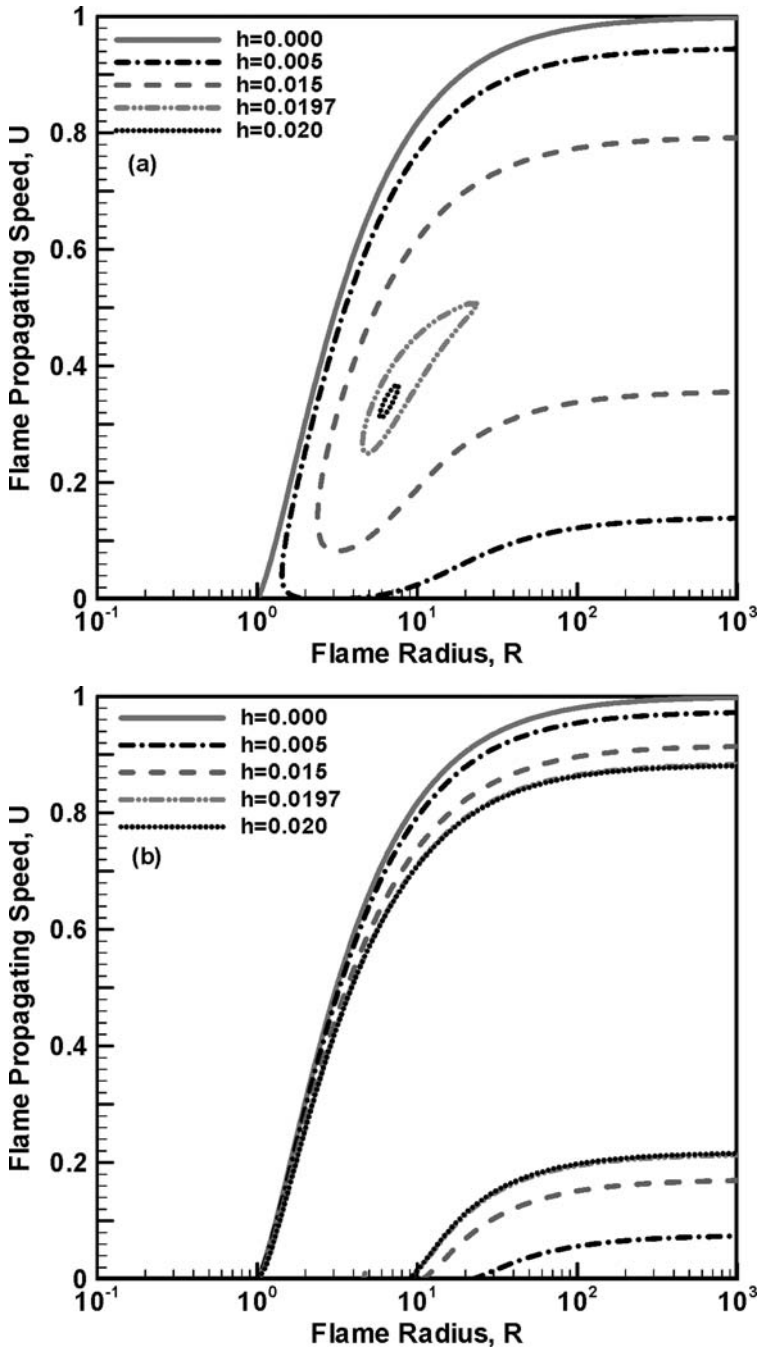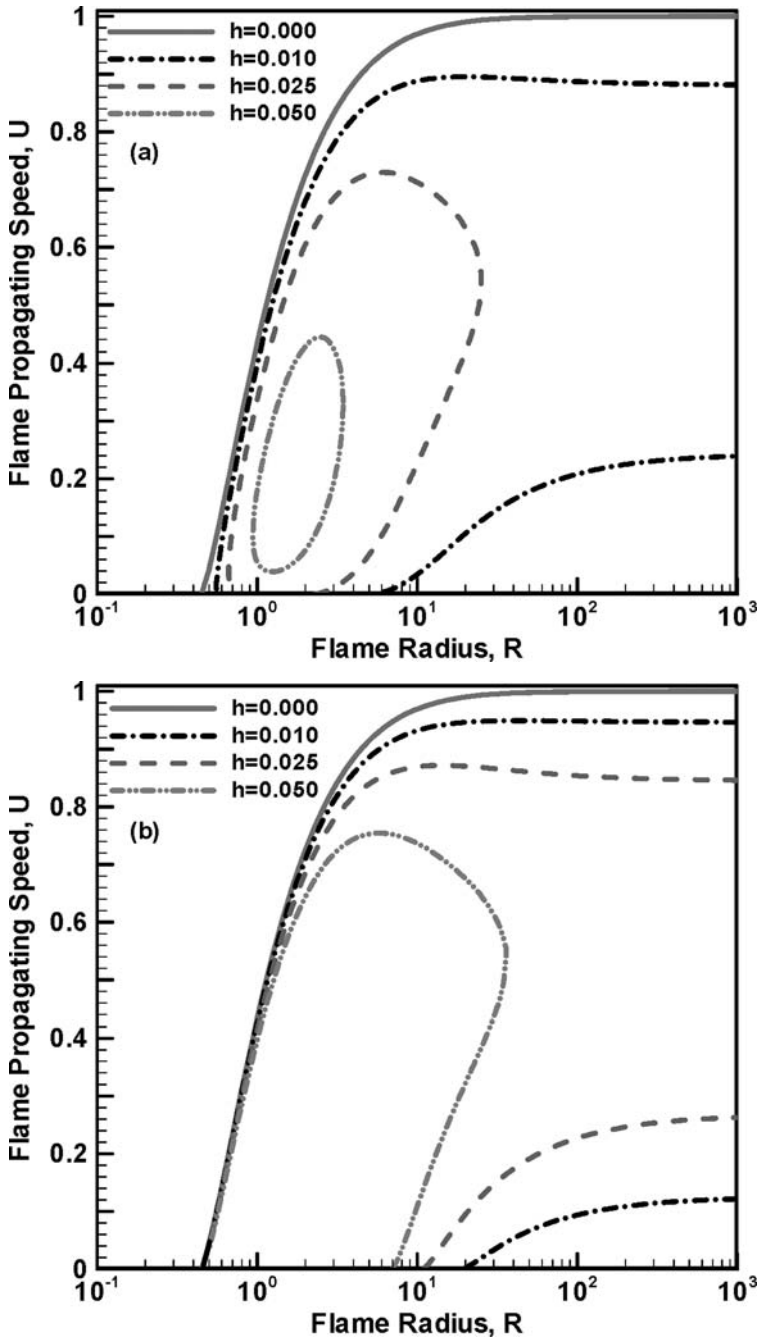
Figure 3.   Flame propagating speed as a function of flame radius for $Le = 1.0$ with different values of radiation heat loss constants: (a), with heat losses in both the burned and unburned zones; (b), with heat loss only in the burned zone.

that in a mixture at $Le = 0.8$, depending on the fuel concentration, there exists five different flames: the flame ball, the outwardly propagating spherical flame, the planar flame, the self-extinguishing flame (SEF) and the isolated self-extinguishing flame (ISEF). Because of the Lewis number effect, the sub-limit SEF and ISEF can exist at much lower concentrations than
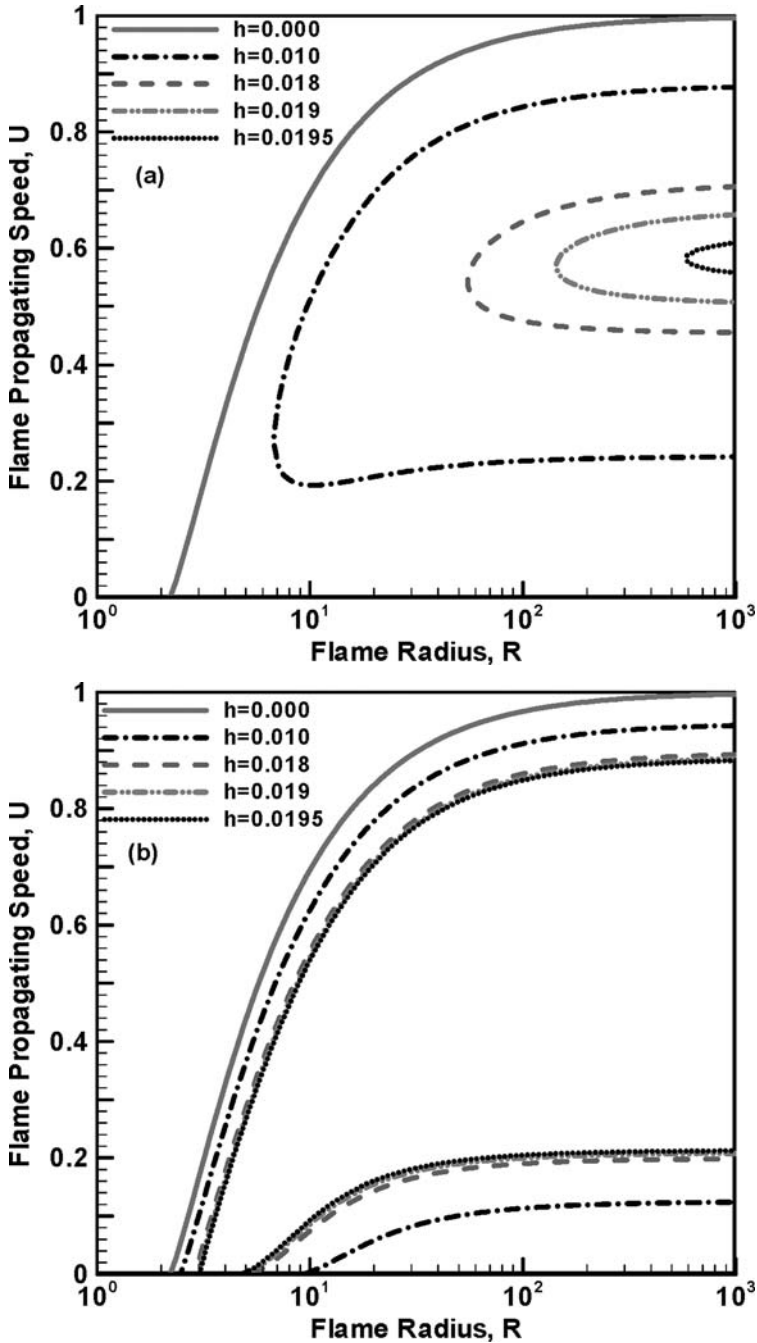
Figure 4. Flame propagating speed as a function of flame radius for $Le = 0.8$ with different values of radiation heat loss constants: (a), with heat losses in both the burned and unburned zones; (b), with heat loss only in the burned zone.

the flammability limit of the planar flame. In addition, stationary flame balls start to appear at small radiation heat losses. These results are consistent with the experimental observation [1, 12–15]. At $Le = 1.2$, figure 5(a) shows that neither flame ball nor sub-limit SEF or ISEF exist. At large radiation heat loss or low fuel concentration, a flame does not exist because of the

Figure 5. Flame propagating speed as a function of flame radius for $Le = 1.2$ with different values of radiation heat loss constants: (a), with heat losses in both the burned and unburned zones; (b), with heat loss only in the burned zone.

combined effect of radiation heat loss in the unburned gas and of the flame stretch. Obviously, the predictions without inclusion of radiation heat loss in the unburned zone [figures 4(b), 5(b)] do not correctly predict this phenomenon. For example, figure 5(b) shows that flame balls exist at all fuel concentrations. This is contrary to experimental observation.
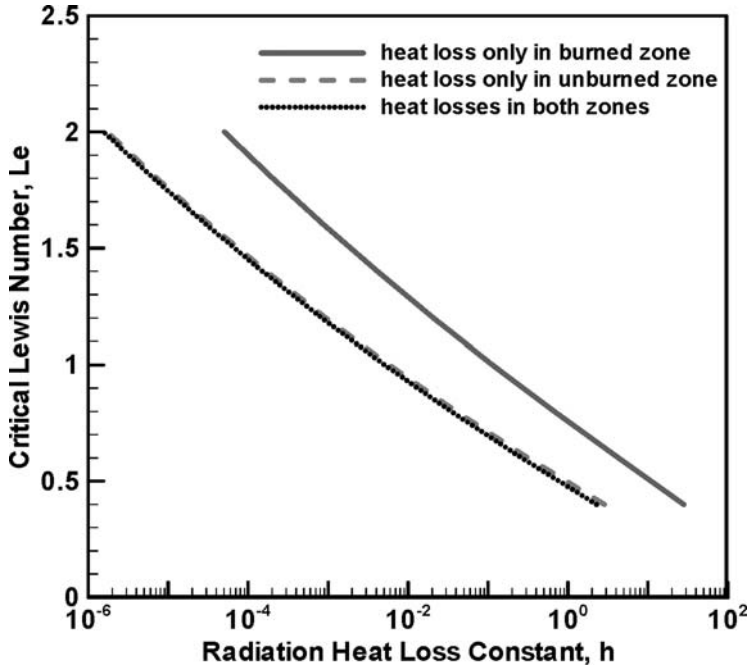
Figure 6.   The dependence of critical Lewis number above which no solution exists for stationary flame ball for a given heat loss constant.

The effects of radiation heat loss on the critical Lewis number below which a quasi-steady state flame ball solution exists are shown in figure 6 for different radiation models. It is seen that for a large radiation heat loss constant, stationary flame balls exist only for small Lewis number, which is consistent with the experimental results in microgravity [1, 12–15]. The importance of radiation heat loss in the unburned zone can also be observed. It is seen that the effect of radiation heat loss on the critical Lewis number for flame ball is dominated by the heat loss in the unburned zone. This conclusion is different from the previous studies in which the radiation heat loss in the unburned region was often ignored. This is because the flame ball size is very small and the diffusion zone is very broad at zero and small flame speed. As a result, the radiation heat loss in the burned zone plays a negligible role in affecting the critical Lewis number.

3.5   *Effect of ignition energy on flame initiation*

We now consider the case in which an external energy flux is deposited in the centre of quiescent mixture and examine how the ignition energy affects the flame diagram and the transition trajectory.

In the quasi-steady model, the ignition energy Q is modelled as a boundary condition (related discussions are presented at the end of this section), that is

$$r^2 \partial T / \partial r |_{r=\varepsilon} = -Q \text{ with } \varepsilon \to 0 \tag{25}$$

The fuel mass fraction distribution is the same as that obtained in section 3.1 and the temperature distribution in the burned gas region ($0 \le r \le R$) is given by

$$T(r) = T_0(r) + Q \cdot T_Q(r) \tag{26}$$

where $T_0(r)$ is the solution in the case of $Q = 0$ [equations (12) and (13)] and $T_Q(r)$ is the temperature increase caused by the external ignition power

$$T_Q(r) = \begin{cases} \displaystyle\int_r^R \frac{e^{-U\tau}}{\tau^2} d\tau & \text{if } h_1 = 0 \\ e^{-0.5(U+k_1)r}\left[C_1 \cdot G\left(-k_1 r, \frac{U}{k_1}, -\frac{U}{k_1}\right) + C_2 \cdot F\left(k_1 r, \frac{U}{k_1}, -\frac{U}{k_1}\right) \right] & \text{if } h_1 \neq 0 \end{cases}$$
(27)

with

$$C_1 = \left[\varepsilon^2 \frac{U + k_1}{2} G(-k_1\varepsilon, U/k_1 - U/k_1) + \varepsilon^2 k_1 G(-k_1\varepsilon, 1 + U/k_1 - U/k_1) \right]^{-1}$$

and

$$C_2 = -C_1 \cdot G(-k_1 R, U/k_1 - U/k_1)/F(k_1 R, U/k_1 - U/k_1).$$

By using the jump relations given by equation (6), the flame speed equation can be obtained as

$$\Omega \cdot T_f + \Omega_Q \cdot Q = \frac{1}{Le} R^{-2} e^{-ULeR} \Big/ \int_R^\infty \tau^{-2} e^{-ULe\tau} d\tau = \exp\left[\frac{Z}{2} \frac{T_f - 1}{\sigma + (1 - \sigma)T_f} \right]$$
(28a)

where Ω is given by equation (14b) and

$$\Omega_Q = \begin{cases} -R^{-2} e^{-UR} & \text{if } h_1 = 0 \\ k_1 e^{-0.5(U+k_1)R}\left[-C_1 \cdot G\left(-k_1 R, 1 + \frac{U}{k_1}, -\frac{U}{k_1}\right) \right. & \text{if } h_1 \neq 0 \\ \left. + C_2 \cdot F\left(k_1 R, 1 + \frac{U}{k_1}, -\frac{U}{k_1}\right) \right] \end{cases}$$
(28b)

The effect of ignition power and Lewis number on flame transition can be studied by solving equation (28) numerically. Figures 7 to 9 show the flame speed as a function of flame radius with different values of ignition power, radiation heat loss constant, and Lewis number. Figure 7(a) shows the results for $Le = 1.0$ and $h = 0$. The solid line ab shows the result of zero ignition energy ($Q = 0$) which is the same as that in figure 3(a). In this case, the outwardly propagating spherical flame only exists beyond a finite flame radius $R_b = 1.0$. When an external energy is deposited, it is seen that the flame transition trajectory is changed. At a low ignition energy of $Q = 0.05$, owing to the increase of flame temperature, the travelling flame branch ab is extended to branch ac and the critical flame initiation radius is reduced to $R_c = 0.72$. At the same time, a new branch (ignition kernel) de is formed at small radius and quenches as it grows. Therefore, flame initiation is not successful. However, by increasing the ignition power to $Q = 0.092$, a new ignition kernel branch fg starts to merge with the travelling flame branch ag, indicating that an outwardly propagating spherical flame can be successfully initiated via the flame transition curve fga. Therefore, we can define the critical ignition power ($Q_C = 0.092$) above which the flame kernel branch always merges with the travelling flame branch.

Figure 7(b) shows the results of non-adiabatic flame evolution diagram for $Le = 1.0$ and $h = 0.01$. Unlike the adiabatic case, no flame ball solution exists and the outwardly propagating spherical flame only exists at a much larger flame radius with a finite flame speed due to the effects of radiation heat loss. When ignition energy is deposited, the new flame kernel branch starts to merge with the travelling flame branch at $Q = 0.107$ and forms three new flame branches, a fast flame transition branch dja and an isolated slow branch ic and an ISEF branch egh. As the ignition power increases, the ISEF branch degenerates and the fast transition branch becomes more monotonic, indicating a successful flame transition from ignition kernel to a
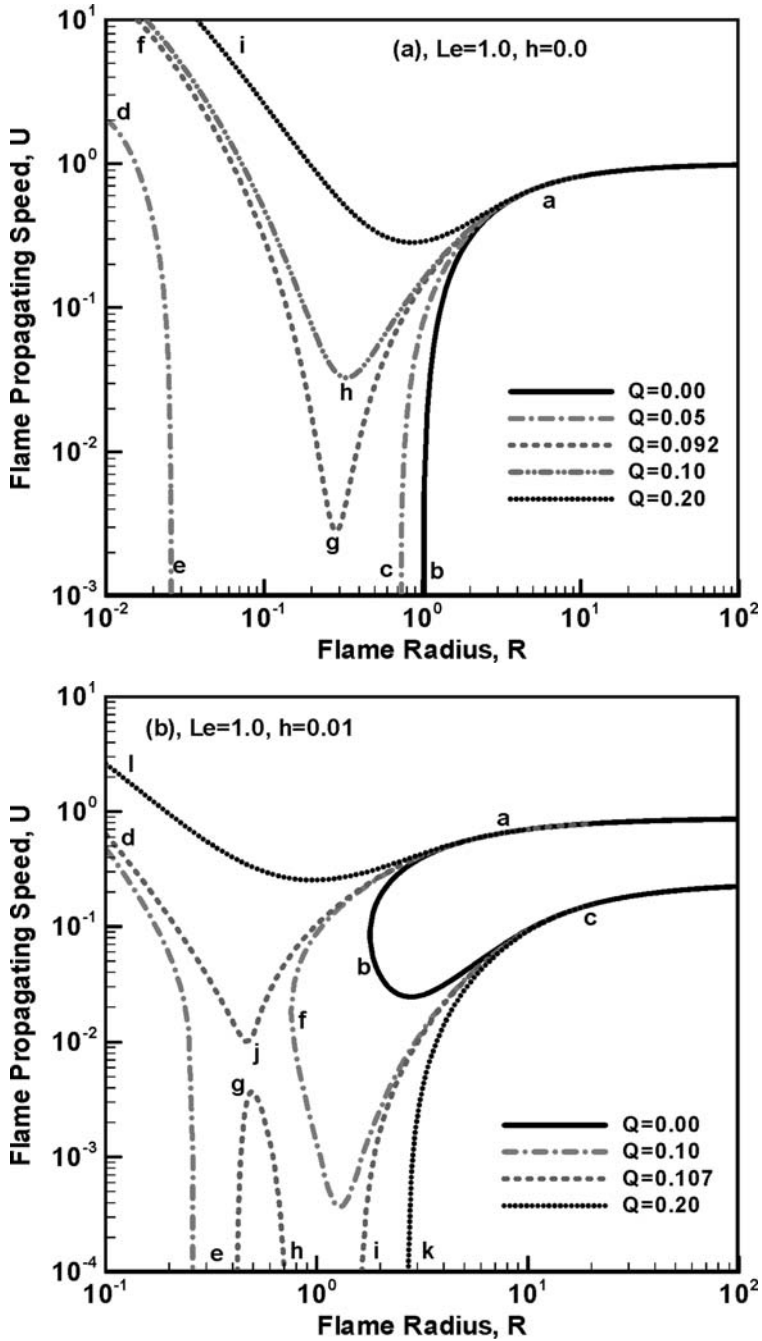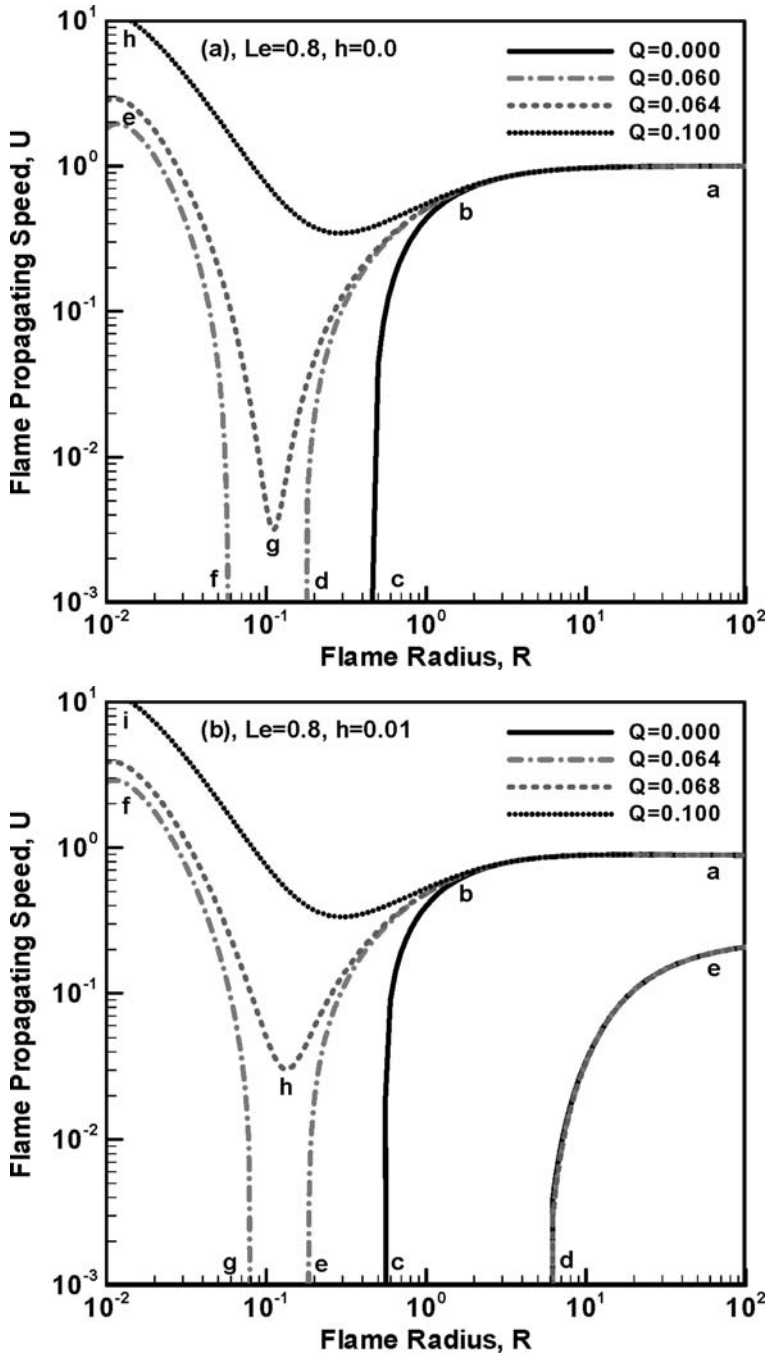
Figure 7. Flame propagating speed as a function of flame radius with different values of ignition power for *Le* = 1.0: (a), *h* = 0.0; (b), *h* = 0.01.

travelling flame. Note that the radiation heat loss not only changes the flame bifurcation but also significantly increases the critical ignition radius (from $R_f = 0.3$ to 0.6) and the critical ignition energy (from $Q = 0.092$ to 0.107). Therefore, the adiabatic model does not adequately describe the flame initiation trajectory. This conclusion is different from that of a previous study [22].

Figure 8. Flame propagating speed as a function of flame radius with different values of ignition power for $Le =$ 0.8: (a), $h = 0.0$; (b), $h = 0.01$.

The adiabatic and non-adiabatic flame trajectory with external ignition energy for $Le = 0.8$ and 1.2 are shown in figures 8 and 9. For the case of small Lewis number (figure 8), owing to the Lewis number effect, the critical ignition radius becomes much smaller and the critical ignition power decreases. Moreover, the radiation effect becomes weaker with the decrease of
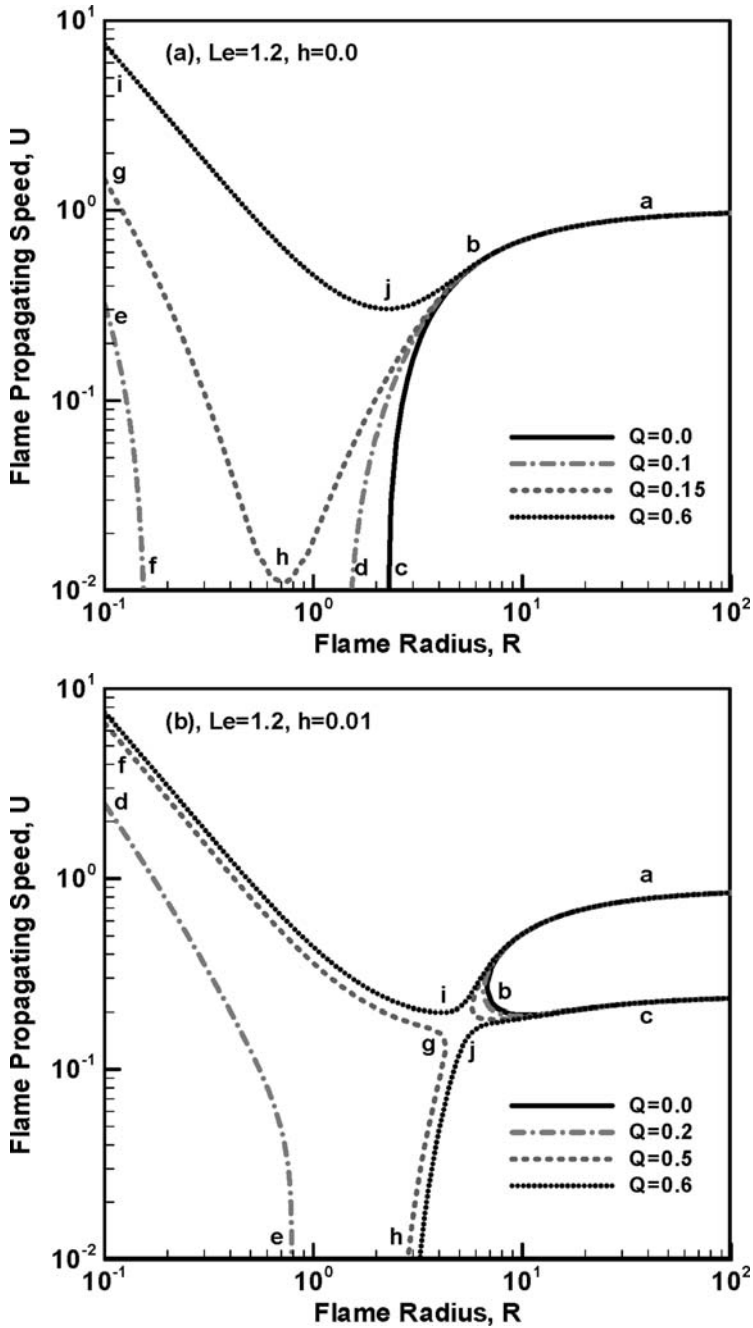
Figure 9. Flame propagating speed as a function of flame radius with different values of ignition power for $Le = 1.2$: (a), $h = 0.0$; (b), $h = 0.01$.

Lewis number. However, at a large Lewis number (figure 9), both the critical ignition radius and the critical ignition power significantly increase. In particular, the adiabatic model [figure 9(a)] not only does not predict a correct flame bifurcation but also fails to predict the size of critical ignition kernel. This conclusion has a significant implication for the gasoline spark ignition process, particularly with CO_2 recirculation.
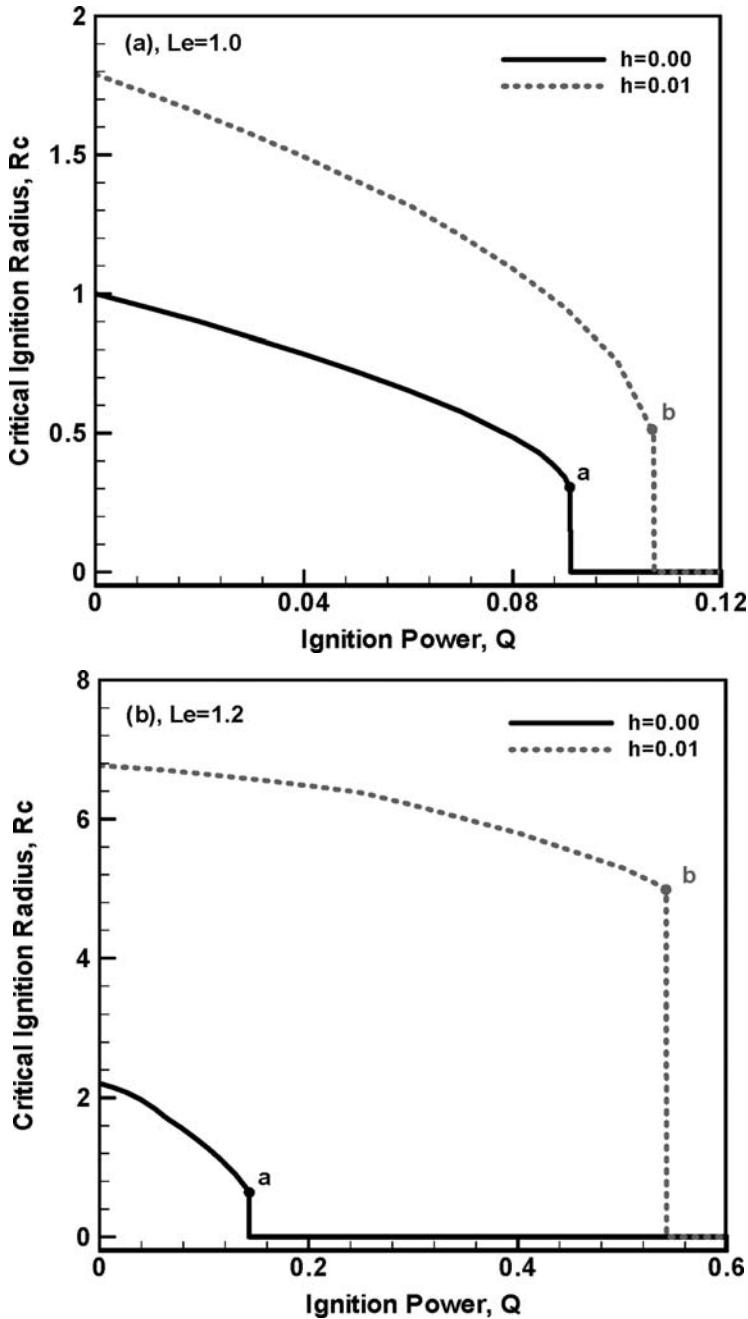
Figure 10. Critical ignition radius with respect to ignition power for adiabatic and non-adiabatic cases: (a), $Le = 1.0$; (b), $Le = 1.2$.

Figure 10 shows the comparison of the critical ignition radius for adiabatic and non-adiabatic flames at $Le = 1.0$ and 1.2, respectively. For $Le = 1.0$, it is seen that for both cases, the critical ignition radius decreases with the increase of ignition power. However, the critical ignition radius for radiating flames is much greater than that of adiabatic flames. When the ignition power is larger than the critical ignition power (Q_a and Q_b), the critical ignition radius goes

to zero, which means that outwardly propagating spherical flame can be successfully initiated from the centre. For $Le = 1.2$, the increase of the critical ignition radius owing to radiation heat loss becomes more profound. In addition, the ratio of critical ignition power between the radiative and adiabatic cases also becomes much larger.

The critical ignition power as a function of Lewis number for adiabatic and non-adiabatic cases is shown in figure 11(a). It is seen that when Lewis number is smaller than 0.8, the critical ignition power for adiabatic and non-adiabatic cases is nearly the same. However, as the Lewis number increases the dependence becomes significantly different. For the adiabatic mixture, the logarithm of critical ignition power only increases linearly with the increase of Lewis number. However, for the radiative mixture, the dependence of the critical ignition energy can be divided into three different regimes: a linear region at small Lewis numbers ($Le < 1$); a nonlinear region at intermediate Lewis numbers ($1 < Le < 1.6$); and a linear region at high Lewis numbers ($Le > 1.6$). The appearance of the nonlinear region is owing to the coupling of the radiation heat loss from the unburned region and the Lewis number effect [figure 11(b)]. Therefore, the radiation heat loss from unburned gas region significantly affects the ignition energy. The present results have a strong relevance in ignition enhancement in internal combustion engines involving natural gas and large hydrocarbon fuels ($Le > 1$).

Note that ignition is an essentially transient process. Depending on the relative magnitude of characteristic times of external heating, chemical reaction, travelling acoustic wave and heat conduction, there are fast-nondiffusive-ignition [25] and thermal-diffusive-ignition [26]. In the current study, the constant density assumption is used and the acoustic effect is neglected because its timescale is far shorter than the thermal diffusion timescale. Therefore, only the thermal-diffusive-ignition is investigated here. It is reasonable because in the practical device the initial flame kernel size is much smaller than the volume of combustion chamber so that the pressure increase can be neglected. Unlike the work of Vázquez-Espí and Liñán [26], in which the unsteady-diffusion-reaction equations similar to equation (1) were solved numerically and radiation heat loss was not considered, here we present a general theory [equation (28)] based on the quasi-steady assumption in which radiation heat loss is included. The shortcoming of current analysis is that the ignition energy deposition is modelled as a boundary condition [equation (25)]; while in practice it should be resolved in time and space. The employment of such a steady state energy deposition is for the purpose to seek analytical solution. However, this simplification does not prevent the model from producing qualitatively correct results. It will be shown in the next section that the results from the current theoretical analysis based on the quasi-steady assumption agree well with those from fully transient numerical simulations.

4. Numerical modelling of the unsteady effects

In order to confirm the validity of the quasi-steady state assumption used in the previous analysis, we performed numerical simulations of the time-dependent flame initiation problem. The non-dimensional form of equations (1a) and (1b) under constant density assumption is solved numerically by means of an implicit finite volume method. To numerically resolve the moving flame front, a ten-level adaptive grinding algorithm has been developed [27]. The mesh addition and removal are based on the first and second order gradients of the temperature and reaction rate distributions. Uniform grids of 0.00125–0.01 (length normalized by flame thickness) are used in the reaction zone and kept moving with the flame front. The following finite reaction rate is used in the numerical simulation

$$\omega = \frac{1}{2Le} \cdot Y \cdot Z^2 \cdot \exp\left[\frac{Z(T-1)}{\sigma + (1-\sigma)T}\right] \tag{29}$$
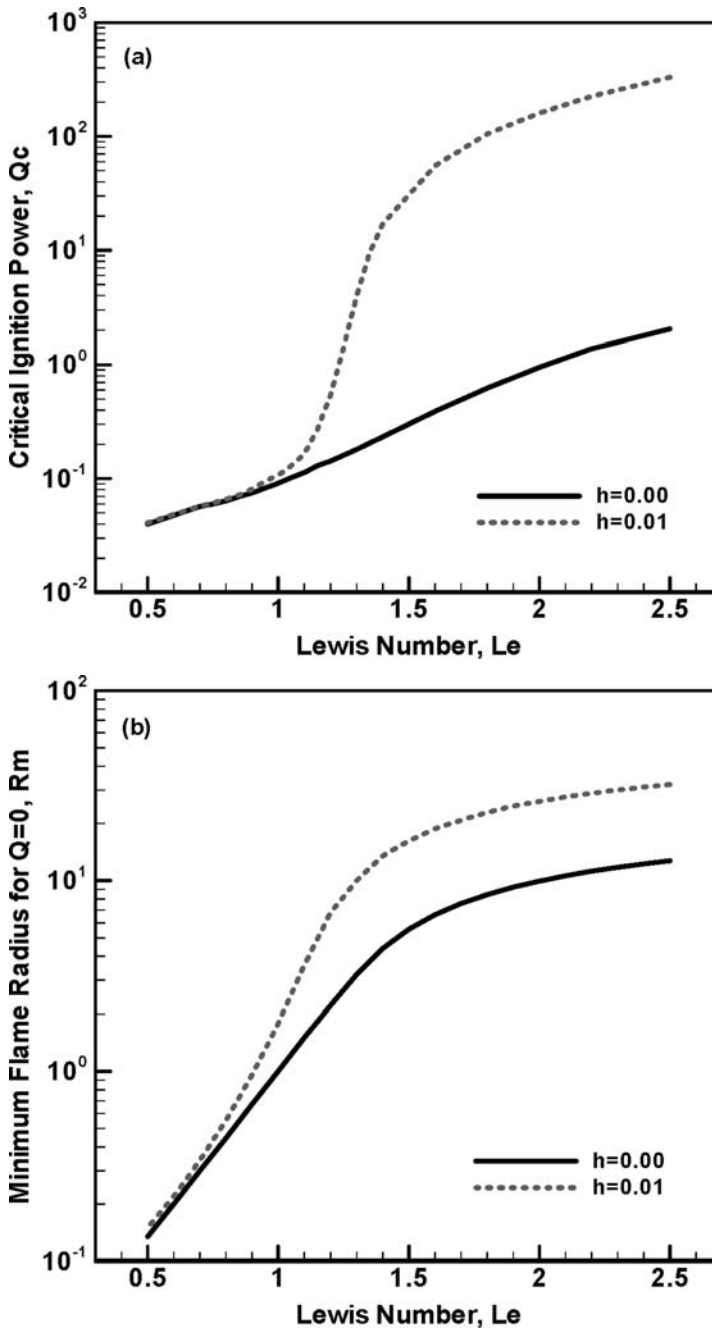
Figure 11. (a) Critical ignition power with respect to Lewis number for adiabatic and non-adiabatic cases; (b) smallest flame radius with respect to Lewis number for adiabatic and non-adiabatic cases without ignition power.

The boundary conditions are the same as those given by equations (7a) and (7c). With an initial uniform temperature and fuel mass fraction distribution of $T(r) = 1 - Y(r) = 0$, the unsteady flame initiation problem is resolved.

To justify the validity of the quasi-steady state assumption used in theoretical analysis, flame speeds at different flame radii predicted from theoretical analysis are compared with
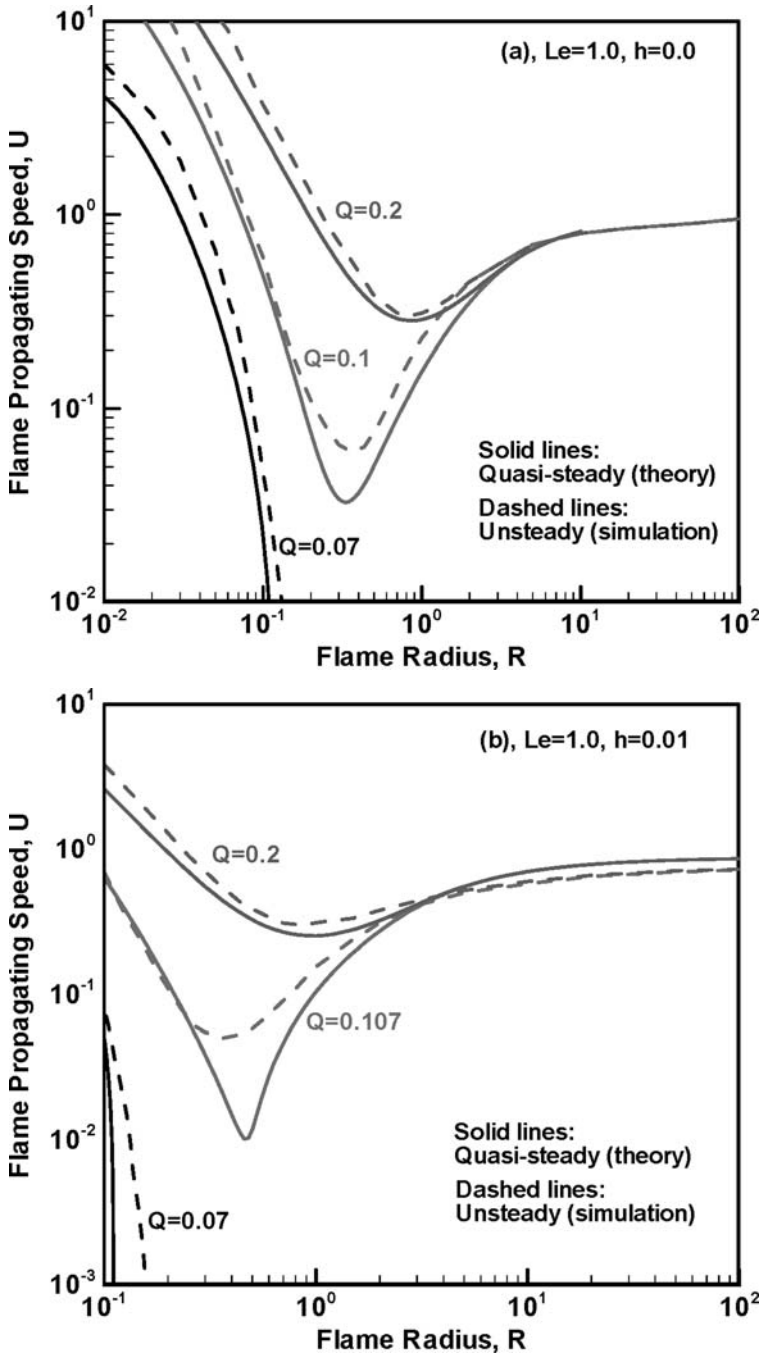
Figure 12. Comparison of flame propagating speeds predicted by numerical simulation and theoretical analysis for $Le = 1.0$: (a), $h = 0.0$; (b), $h = 0.01$.

those from numerical simulations, in which the flame propagating speed is calculated from the flame front history, i.e. $U = dR/dt$, where the flame front is defined as where the maximum heat release appears. Figure 12 shows the results for $Le = 1$ without and with radiation heat loss. It is seen that the results from theory agree reasonably well with those from the unsteady

simulations. As with most other studies on flame dynamics, the unstable branches predicted by theoretical analysis as labelled by *egh* and *kc* in figures 7(b) could not be recovered from numerical simulations. Comparisons for other Lewis numbers without and with radiation heat loss are also made. The qualitatively agreement is obtained.
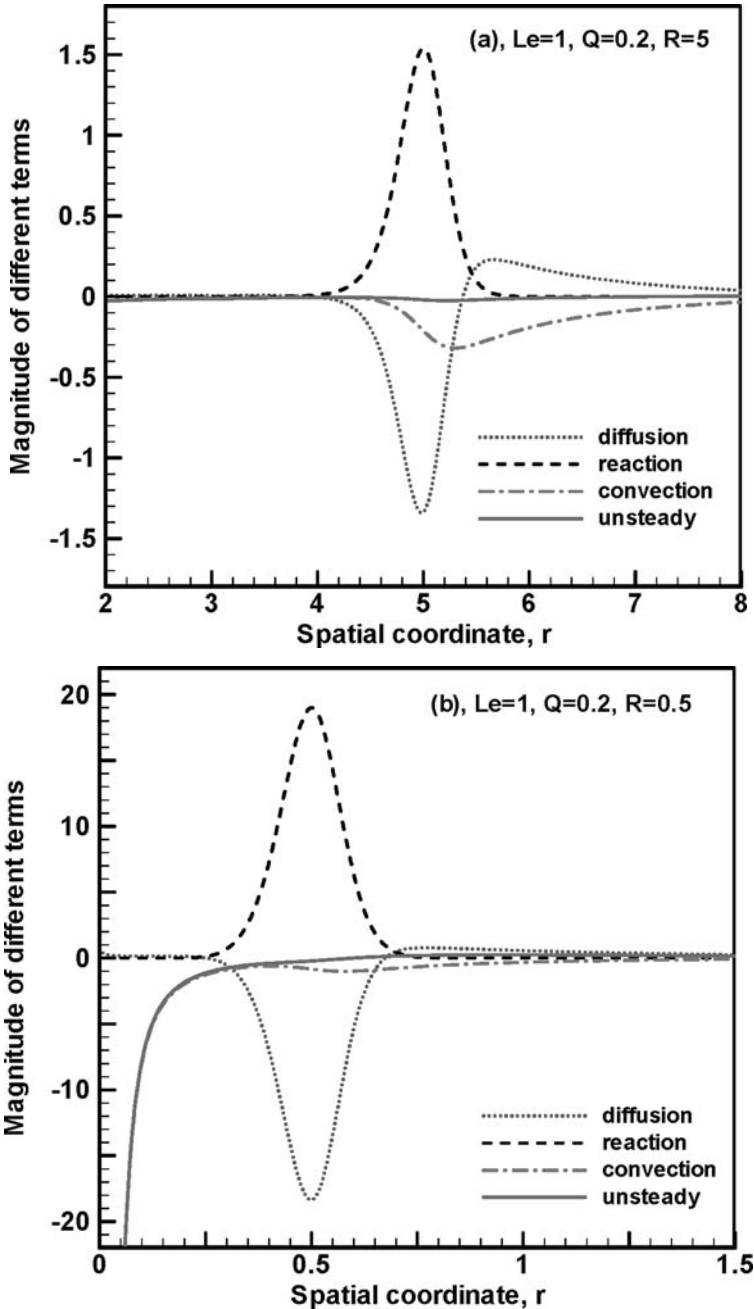

Figure 13. The unsteady term ($\partial T/\partial t$), convection term ($U\partial T/\partial r$), diffusion term ($\partial(\partial T/r^2\partial r)/r^2\partial r$), and reaction term ($\omega$) in equations (3a) predicted from numerical simulation for flames at different flame radii with $Le = 1.0$ and $Q = 0.2$:, (a), $R = 5.0$; (b), $R = 0.5$.

In order to evaluate quantitatively the magnitude of the unsteady term, the numerical results from unsteady simulation were transformed into the flame front attaching coordinate (in which theoretical analysis was carried out). The magnitudes of unsteady term ($\partial T/\partial t$), convection term ($U\partial T/\partial r$), diffusion term ($\partial(\partial T/r^2\partial r)/r^2\ \partial r$) and reaction term ($\omega$) in equations (3a) and (3b) are evaluated and compared in the transformed coordinate. The importance of the unsteady effects is shown by comparing the unsteady term with other terms. Figure 13 shows the distributions of the unsteady, convection, diffusion, and reaction terms in energy equation (3a) for flames at different flame radii with $Le = 1.0$ and $Q = 0.2$. When the flame radius is large, $R = 5.0$ in figure 13(a), the unsteady term is one order smaller than all other terms, therefore it is negligible. For cases of larger flame radii, the unsteady term becomes much smaller. Therefore it is reasonable to employ the quasi-steady state assumption. When the flame radius is small, $R = 0.5$ in figure 13(b), the diffusion and reaction terms will dominate, while the unsteady and convection terms are relatively small near the flame front. However, near the centre where energy deposition exists, the unsteady term is very large and is balanced by the convection term. This is because the energy deposition in the centre (modelled as a boundary condition) is moving away from the flame front in the flame front attaching coordinate.

Furthermore, to investigate the effect of the timescale of energy deposition on the flame trajectory, we compared the flame-front trajectories obtained from time-dependent numerical computations with different duration time (ts) at a given energy flux (Q). In numerical simulation, the energy flux Q at the boundary [equation (7a)] is set to zero when the time is greater than the duration time (ts). Figure 14 shows the results for $Le = 1.0$, $h = 0.01$ and $Q = 0.2$. It is seen that the flame initiation fails when the duration is too small. However, when $ts \geq 6.5$ the flame-front trajectory (which is the same as that of $ts = 6.5$) is not affected by the change of the timescale of energy deposition. Therefore in this case, the duration must be
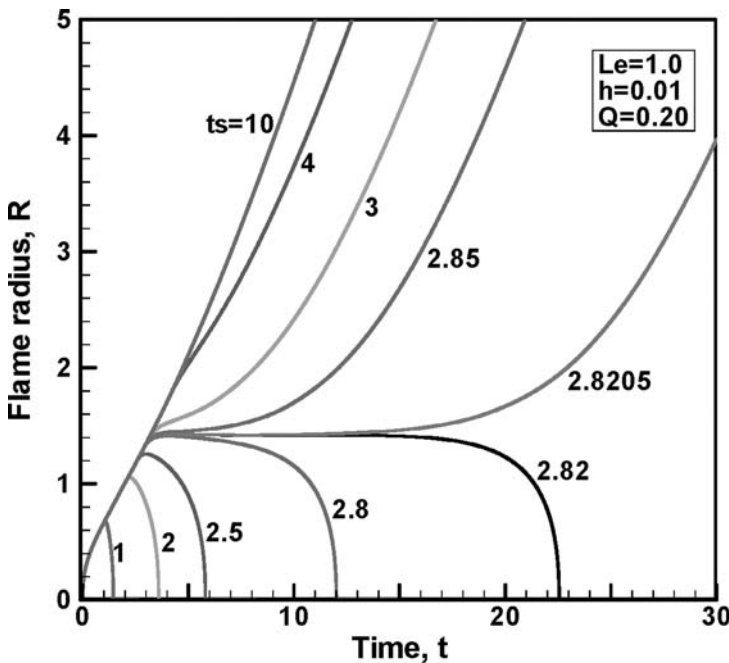

Figure 14. Flame-front trajectories obtained from numerical computations with different duration time (ts) at a given energy flux ($Q = 0.2$) for $Le = 1.0$ and $h = 0.01$.

large than 6.5 (time normalized by flame thickness divided by planar flame speed) to make the quasi-steady model consistent. Similar results were also presented in He [22].

5. Conclusions

An analytical solution to describe the flame regimes and transitions between the flame kernel, the flame ball, the self-extinguishing flame, the outwardly propagating spherical flame and the propagating planar flame is obtained. The present study extends the previous results by bridging the theories of non-adiabatic stationary flame balls and travelling flames and allowing rigorous consideration of radiation heat losses in both the burned and unburned zones. The results show that the effects of radiation heat loss play a very important role on flame regimes, transition, and critical ignition radius and power and therefore it should not be neglected.

It is shown that radiation heat losses from the unburned and burned zones play different roles in affecting flame propagating speed. With the increase of flame radius, the radiation heat loss from the burned zone increases, while the radiation heat loss from the unburned zone decreases. As a result, there is a peak radiation loss at an intermediate flame radius, which dramatically affects the flame regimes and critical flame initiation parameters. It is also found that the radiation heat loss from the unburned zone results in a new flame regime: the isolated self-extinguishing flame with two radiation extinction limits respectively at small and large flame radius. In addition, it is shown that the critical Lewis number for the stationary flame ball is dominated by the heat loss from the unburned gas.

The results also show that radiation heat loss significantly affects the transition history of flame initiation with external energy deposition. The critical radius of successful flame initiation for radiative flames is much larger than that of adiabatic flames. Furthermore, this difference increases dramatically with the increase of the mixture Lewis number. It is shown that, owing to the coupling of radiation heat loss and the Lewis number effect, the dependence of the minimum ignition energy on Lewis number has three different regimes. At intermediate Lewis numbers, the results show that the minimum ignition energy increases exponentially with the increase of the Lewis number. The prediction agrees qualitative well with the unsteady numerical simulations. These results could have a significant impact on technological developments for ignition control of internal combustion engines.

Acknowledgement

References

[1] Ronney, P.D., 1988, On the mechanics of flame propagation limits and extinguishment processes at microgravity. *Proceedings of the Combustion Institute,* **22**, 1615–1623.
[2] Ju, Y., Maruta, K. and Niioka, T., 2001, Combustion limits. *Applied Mechanical Review*, **54**, 257–277.
[3] He, L. and Law, C.K., 1999, On the dynamics of transition from propagating flame to stationary flame ball. *AIAA* 99–0325.
[4] Spalding, D.B., 1957, A theory of inflammability limits and flame-quenching. *Proceedings of the Royal Society of London, Series A*, **240**, 82–100.
[5] Buckmaster, J., 1976, The quenching of deflagration waves. *Combustion and Flame*, **26**, 151–162.
[6] Ju, Y., Guo, H., Maruta, K. and Liu, F., 1997, On the extinction limit and flammability limit of non-adiabatic stretched methane-air premixed flame. *Journal of Fluid Mechanics*, **342**, 315–334.

 [7] Maruta, K., Yoshida, M., Guo, H., Ju, Y. and Niioka, T., 1998, Extinction of low-stretched diffusion flame in microgravity. *Combustion and Flame*, **112**, 181–187.
 [8] Ju, Y., Guo, H., Liu, F. and Maruta, K., 1999, Effects of the Lewis number and radiative heat loss on the bifurcation and extinction of CH_4/O_2-N_2-He flames. *Journal of Fluid Mechanics*, **379**, 165–190.
 [9] Zel'dovich, Ya. B., Barenblatt, G.I., Librovich, V.B. and Makhviladze, G.M., 1985, *The Mathematical Theory of Combustion and Explosions* (New York: Consultants Bureau).
[10] Deshaies, B. and Joulin, G., 1984, On the initiation of a spherical flame kernel, *Combustion Science Technology*, **37**, 99–116.
[11] He, L. and Clavin, P., 1993, Premixed hydrogen-oxygen flames. Part II: Quasi-isobaric ignition near the flammability limits. *Combustion and. Flame*, **93**, 408–420.
[12] Ronney, P.D. and Wachman, H.Y., 1985, Effect of gravity on laminar premixed gas combustion I: Flammability limits and burning velocities. *Combustion and Flame*, **62**, 107–119.
[13] Ronney, P.D., 1985, Effect of gravity on laminar premixed gas combustion II: Ignition and extinction phenomena. *Combustion and Flame*, **62**, 121–133.
[14] Ronney, P.D., 1990, Near-limit flame structures at low Lewis number. *Combustion and Flame*, **82,** 1–14.
[15] Abbud-Madrid, A. and Ronney, P.D., 1990, Effects of radiative and diffusive transport processes on premixed flames near flammability limits. *Proceedings of the Combustion Institute*, **23**, 423–431.
[16] Buckmaster, J., Joulin, G. and Ronney, P., 1990, The structure and stability of non-adiabatic flame balls. *Combustion and Flame*, **79**, 381–392.
[17] Buckmaster, J., Joulin, G. and Ronney, P., 1991, The structure and stability of non-adiabatic flame balls: II. Effects of far field losses. *Combustion and Flame*, **84**, 411–422.
[18] Wu, M.S., Ronney, P.D., Colantonio, R. and VanZandt, D., 1999, Detailed numerical simulation of flame ball structure and dynamics. *Combustion and Flame*, **116**, 387–397.
[19] Bechtold, J.K., Cui, C. and Matalon, M., 2005, The role of radiative losses in self-extinguishing and self-wrinkling flames. *Proceedings of the Combustion Institute,* **30**, 177–184.
[20] Tse, S.D., He, L. and Law, C.K., 2000, A computational study of the transition from localized ignition to flame ball in lean hydrogen/air flames. *Proceedings of the Combustion Institute*, **28**, 1917–1924.
[21] Yuan, J., Tse, S.D. and Law, C.K., 2002, Dynamics of flame-ball formation from localized ignition: effects of elevated pressure and temperature. *Proceedings of the Combustion Institute*, **29**, 2501–2507.
[22] He, L., 2000, Critical conditions for spherical flame initiation in mixtures with high Lewis numbers. *Combustion. Theory Modelling*, **4**, 159–172.
[23] Joulin, G. and Clavin, P., 1979, Linear stability analysis of non-adiabatic flames: diffusional-thermal model. *Combustion and Flame*, **35**, 139–153.
[24] Frankel, M.L. and Sivashinsky, G.I., 1984, On quenching of curved flames. *Combustion Science and Technology*, **40**, 257–268.
[25] Vázquez-Espí, C. and Liñán, A., 2001, Fast, non-diffusive ignition of a gaseous reacting mixture subject to a point energy source. *Combustion Theory Modelling*, **5**, 485–498.
[26] Vázquez-Espí, C and Liñán, A., 2002, Thermal-diffusive ignition and flame initiation by a local energy source. *Combustion Theory Modelling*, **6**, 297–315.
[27] Chen, Z., Qin, X., Xu, B., Ju, Y. and Liu, F., 2006, Studies of radiation absorption on flame speed and flammability limit of CO_2 diluted methane flames at elevated pressures. *Proceedings of the Combustion Institute*, **31**. In press.